Phase Relationships in the N_2O_3/N_2O_4 System and Crystal Structures of N_2O_3

Jörg Horakh, Horst Borrmann, and Arndt Simon*

Abstract: Mixtures of N_2O_3 and N_2O_4 have been prepared from measured volumes of NO and O_2. Phase relationships in the system N_2O_3/N_2O_4, which depend on the composition of the samples and on the temperature, were studied by the Guinier technique and differential thermal analysis. Single crystals of phases A and B of N_2O_3 were grown in situ on a diffractometer and studied at temperatures between -107 and $-170\,^{\circ}C$ by X-ray diffraction. The structure analysis of A-N_2O_3 (tetragonal, space group $I4_1/a$, $T = -170\,^{\circ}C$, $a = 1625.57(16)$, $c = 880.49(13)$ pm, $Z = 32$, $R1 = 0.051$ for 1030 unique reflections) is hampered by twinning and additional disorder of one of two crystallographically independent molecules. B-N_2O_3 is nicely ordered with one molecule in the asymmetric unit (orthorhombic, space group $P2_12_12_1$, $T = -160\,^{\circ}C$, $a = 506.86(4)$, $b = 647.96(5)$, $c = 863.26(6)$ pm, $Z = 4$, $R1 = 0.023$ for 1352 unique reflections). The most interesting features of the N_2O_3 molecule are its planarity and the extraordinarily long N–N bond (189.0(1) pm).

Keywords
crystal structure · differential thermal analysis · nitrogen oxides · phase transitions · twinning

Introduction

In 1816 Gay-Lussac proposed the existence of "acide pernitreux" consisting of two parts nitrogen and three parts oxygen.[1] Nevertheless, in 1959 the structure of the indigo-blue N_2O_3 was still the subject of discussion.[2] IR,[3] Raman,[4] and NMR[5, 6] experiments indicated the existence of an N–N bond in the condensed and gaseous phases as well as in solution. Microwave spectra revealed some remarkable features of the molecule in the gas phase:[7] N_2O_3 is a planar molecule with an unusually long N–N bond of 186.4 pm, which is even longer than that of N_2O_4.[8] A second isomer of N_2O_3 has been reported,[9] namely, the symmetric molecule O-N-O-N-O, which was obtained by matrix isolation techniques at low temperatures.

Reed and Lipscomb reported the unit cell of N_2O_3 crystals at $-115\,^{\circ}C$ to be tetragonal ($a = 1640$, $c = 886$ pm) and to contain 32 molecules.[10] Diffraction patterns indicated the presence of Laue class $4/mmm$, and space group $I4_122$ was assumed from reflection conditions. However, the structure remained unsolved. Upon cooling below $-125\,^{\circ}C$ the authors observed a transition, which changed the single crystal reflections into a powder pattern.

Earlier we reported on temperature-dependent X-ray investigations of polycrystalline N_2O_3/N_2O_4 samples and the single-crystal structure determination of B-N_2O_3 at $-160\,^{\circ}C$.[11] Depending on temperature and thermal treatment of the samples, we observed six diffraction patterns corresponding to phases A to F, in addition to patterns of the cubic and monoclinic forms of N_2O_4. In order to find suitable conditions for selective crystal growth of phases A and B of N_2O_3, we investigated the phase relationships in the system N_2O_3/N_2O_4 as a function of temperature and composition. Using the modified Guinier technique[12] and differential thermal analysis, we found suitable conditions for growing single crystals of A-N_2O_3, the phase studied by Reed and Lipscomb.[10]

[*] Prof. Dr. A. Simon, J. Horakh, Dr. H. Borrmann
Max-Planck-Institut für Festkörperforschung
Heisenbergstrasse 1, D-70569 Stuttgart (Germany)
Telefax: Int. code + (0711)689-1010

Experimental Section

Materials: The samples were prepared from O_2 (99.998 vol%, Messer Griesheim GmbH, Germany), which was used without purification, and NO (99.8 vol%, Messer Griesheim GmbH, Germany). NO was purified by condensing it at $-196\,^{\circ}C$ as a slightly green solid, and volatile components were removed in a dynamic vacuum. By interrupting cooling for a short period of time, a small quantity of NO was sublimed to a U-trap maintained at $-196\,^{\circ}C$ where it was deposited as a white powder.

Apparatus and Technique: We used a Duran glass vacuum line (Fig. 1) made of tubing of 3–8 mm o.d. Two glass bulbs (Fig. 1, c) with calibrated volumes were joined to the apparatus. Duran glass X-ray capillaries (0.2 mm o.d.) were fused to the vacuum line. In order to avoid grease, which might absorb the gases or react with them, we employed valves with PTFE O-ring fittings (J. Young, Scientific Glassware, Acton, London, England). Valves were used to close off the bulbs or the capillaries as well as the whole apparatus from the high vacuum system (Fig. 1, a). An MKS Baratron type 221A pressure gauge (Fig. 1, d; 0–1400 Pa, MKS Instruments, Andover, MA 01810), in conjunction with the two calibrated volumes, was used to measure gases. Exact gas pressures could be adjusted by means of a PTFE needle valve (Fig. 1, b) connecting the apparatus with the vacuum system. The whole apparatus was dried at 20 °C under vacuum (10^{-6} mbar) for two days.

Preparation of X-ray Samples: Seven samples of N_2O_3/N_2O_4 containing 10–95% N_2O_3 were prepared and investigated. Assuming ideal gas behavior of NO and O_2, the gases were enclosed in the two bulbs at measured pressures. After the apparatus had been evacuated and disconnected from the vacuum line, the reactants were mixed. The resulting gas pressure corresponded to the sum of P_{NO} and P_{O_2}, indicating that no reaction had taken place. Condensation of the mixture by cooling with liquid nitrogen and subsequent evaporation decreased the pressure. After several cycles of evaporation and condensation, no remaining gaseous components could be detected (<0.5 Pa). An explanation for this procedure was given by

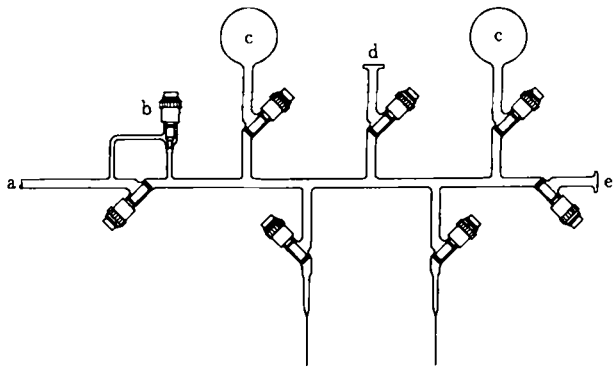

Fig. 1. Apparatus for sample preparation: a) connection to high vacuum or NO; b) PTFE needle valve; c) bulbs with calibrated volumes; d) connection to pressure gauge; e) connection to O_2.

Biltz et al. [14]: by cooling NO/O_2 mixtures with liquid nitrogen, NO is condensed in excess, and layers of different compositions are formed. The evaporation/condensation cycle therefore has to be repeated several times in order to achieve complete reaction. The mixture was condensed at -196 °C into the X-ray capillary to a height of 1–2 cm and sealed with a small flame. The pressure of the remaining gases in the apparatus was ≤ 1 Pa corresponding to $\leq 0.5\%$ of the entire material. The sample was then transferred rapidly from liquid nitrogen to a methylcyclopentane/liquid nitrogen cooling bath (-142 °C). In order to avoid rapid and uncontrolled melting of the substance, which might destroy the capillary, the sample was kept in the cooling bath until its temperature reached -80 °C. After transfer on dry-ice the capillary was glued into a sample holder and mounted on the single-crystal diffractometer or the powder camera, respectively.

Temperature-Dependent X-ray Powder Investigations: Temperature-dependent powder diffraction experiments with Cu($K\alpha_1$) radiation were performed in the temperature range -190 to -100 °C, by using the modified Guinier technique [12]. All samples were warmed to room temperature for some seconds, quenched to the starting temperature, and subsequently investigated at continously adjusted temperatures (0.4–2.5 °C h^{-1}). Above -150 °C the intense lines of the cubic phase of N_2O_4 were observed with all samples. The metastable monoclinic N_2O_4, which transformed to the cubic phase, was occasionally obtained after quenching to -115 °C. Investigations on the phase relationships of N_2O_4[8] show that the temperature range in which this phase can be observed depends on the amount of impurities. The appearance of monoclinic N_2O_4 down to -130 °C is clearly due to its stabilization by the high content of the "impurity" N_2O_3. Characteristic features of the N_2O_3/N_2O_4 system are shown in Figure 2: The diffraction pattern of phase E was observed after shock-cooling to temperatures below -150 °C. Upon heating, the patterns of B-N_2O_3 and cubic N_2O_4 developed simultaneously at -150 °C. Phase B of N_2O_3 transformed at -125 °C to phase A of N_2O_3. The pattern of the latter could be identified by comparison with a powder pattern calculated from structure factors given by Reed and Lipscomb [10].

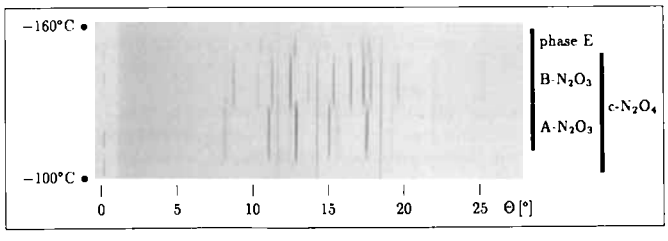

Fig. 2. ΔT-Guinier diagram of a shock-cooled sample from -160 to -100 °C (1.3 °C h^{-1}, 1.0 mm h^{-1}; Cu($K\alpha_1$) radiation).

Samples with N_2O_3 concentrations higher than 70% did not form A-N_2O_3 from the melt. However, this phase could be obtained in these samples when B-N_2O_3 was heated above -130 °C. For samples containing 20–40% N_2O_3, A-N_2O_3 crystallized more readily than B-N_2O_3. Samples cooled to -160 °C showed (besides cubic N_2O_4, which was observed over the whole temperature range) the presence of phase A, which transformed to phase B at -140 °C and back to A-N_2O_3 at -130 °C. Sometimes an additional phase F was observed for all N_2O_3 concentrations. When samples were cooled from a starting temperature of -115 °C, phase F formed at about -135 °C, provided that no other phase of N_2O_3 had already crystallized. When heated, phase F transformed at -150 °C to B-N_2O_3.

Differential Thermal Analysis (DTA): N_2O_4 was condensed at -78 °C into a Duran-glass tube of 3 mm o.d. To maximize the amount of N_2O_3 in the reaction product, a P_{NO} of 1 bar was maintained in the apparatus. After several hours at -40 to -70 °C with intermittant short warming periods to room temperature the substance changed color from greenish blue to dark blue. The tube was sealed at -100 °C under 1 bar of NO, quenched with liquid nitrogen, and transferred to the DTA apparatus equipped with a nitrogen-stream low-temperature device [13], which allows temperatures to be lowered down to -180 °C. Heating at a rate of 40 °C h^{-1} from -165 to -90 °C gave rise to a strong and sharp exothermic effect at -150 °C, to a weaker and broader endothermic effect at -125 °C, and to the strong endothermic effect of eutectic melting at -107 °C. The exothermic effect could be obtained only after shock cooling with liquid nitrogen, while the phase transition at -125 °C is enantiotropic since the low-temperature phase was recovered after annealing at -160 °C for some hours.

Crystal Growth of A-N_2O_3: Crystals of phase A of N_2O_3 were grown in situ on the diffractometer. The sample (40% N_2O_3) crystallized at -120 °C as a blue solid, which yielded powder patterns of cubic N_2O_4 and A-N_2O_3 on rotation photographs. Recrystallization of N_2O_3 was effected by partial melting of the sample and subsequent cooling at 1 °C h^{-1}. This procedure was controlled by measuring the intensities of strong reflections. After several heating and cooling cycles, rotation and oscillation photographs showed crystals of A-N_2O_3 to be present; in addition, smaller fragments of other crystals and powder lines of cubic N_2O_4 were invariably observed.

X-Ray Single-Crystal Data Collection and Structure Analysis for A-N_2O_3: Data collection was performed on a Syntex $P2_1$ diffractometer equipped with a graphite monochromator (Mo($K\alpha$) radiation, $\lambda = 71.073$ pm) and a nitrogen-stream low-temperature device. Temperature fluctuations, monitored by a Pt100 resistance thermometer, were less than ± 0.5 K over a period of days during data collection and could be stabilized to ± 0.1 K during crystal growth.
X-ray data are based on two crystal specimens (crystals **1** and **2**) with diameters of 0.1–0.2 mm. We collected data for crystal **1** at -115, -120, and -170 °C, and for crystal **2** at -120 °C. Unit-cell dimensions were obtained by least-squares refinement of setting angles for 50 reflections with 2θ values of 20–30°. Intensities were measured in $\omega/2\theta$ mode with a variable scan width from $2\theta(\alpha_1)-A$ to $2\theta(\alpha_2)+A$ for each peak and a background-to-scan-time ratio of 0.5. Optimal values for A were found to be 0.6–1.0° by inspection of profiles of selected reflections. We used scan speeds of 1.1–29.3° min^{-1}, depending on the I measured by prescans. The intensities of two standard reflections were monitored every 73 reflections for crystal **1** and every 48 reflections for crystal **2**; no significant decay was observed during the course of data collection. Data processing included corrections for Lp effects but no correction for absorption. Details of data collection and refinement for crystal **1** at -170 °C are given in Table 1 [15]. Structure solution in space group $I4_1/a$ by direct methods was performed with the program system SHELXTL-PLUS [16]. All structures were refined on F^2 with the program SHELXL-93 [17]. Isotropic extinction effects, corrected by least-squares refinement were negligible for both crystal specimens. Positional and displacement parameters obtained for crystal **1** at -170 °C are given in Table 2.

Table 1. Crystallographic data for A-N_2O_3 and B-N_2O_3.

	A-N_2O_3	B-N_2O_3
M_r	76.012	76.012
space group	$I4_1/a$	$P2_12_12_1$
a/pm	1625.57(16)	506.86(4)
b/pm	a	647.96(5)
c/pm	880.49(13)	863.26(6)
$V/10^6$ pm^3	2326.68(57)	283.52(4)
Z	32	4
T/°C	-170	-160
ρ_{calcd}/g cm^{-3}	1.736	1.781
$\lambda(Mo_{K\alpha})$/pm	71.073	
$\mu(Mo_{K\alpha})$/cm^{-1}	1.9	1.9
$F(000)$	1216	152
no. of measured reflections	3233	2723
no. of unique reflections	1030	1352
no. of refined parameters	101	47
R_{int} (all data) [a]	0.028	0.014
$R1$ (all data) [b]	0.051	0.023
$wR2$ (all data) [c]	0.108	0.0491
extinction corr., x [d]	0.0001	0.016
goodness of fit, S	1.05	0.961

[a] $R_{int} = \sum|F^2-(F^2)_{mean}|(\sum F^2)^{-1}$. [b] $R1 = \sum||F_o|-|F_c||(\sum|F_o|)^{-1}$. [c] $wR2 = [\sum w(F_o^2-F_c^2)^2(\sum w(F_o^2)^2)^{-1}]^{1/2}$. [d] $F^* = F_c(1+0.001\,x\,F_c^2\,\lambda^3\sin^{-1}2\theta)^{-1/4}$.

0947-6539/95/0106-0390 $ 30.00+.25/0 Chem. Eur. J. 1995, 1, No. 6

Table 2. Fractional atomic coordinates and equivalent isotropic displacement parameters (pm^2) for A-N_2O_3 at −170 °C.

atom	x/a	y/b	z/c	U(eq) [a]
N1a	0.16326(16)	0.59623(16)	−0.23707(32)	576.5(65)
N2a	0.04780(14)	0.62088(13)	−0.24489(29)	457.0(58)
O1a	0.18534(15)	0.62892(16)	−0.33536(31)	746.1(71)
O2a	0.02654(14)	0.66219(13)	−0.34875(29)	715.3(71)
O3a	0.00648(15)	0.59107(16)	−0.14707(27)	780.5(76)
N1b	0.37690(31)	0.67795(16)	0.01044(65)	362.6(95)
N1b'	0.35693(39)	0.67698(17)	−0.02742(67)	362.6(95)
N2b	0.37841(14)	0.56137(12)	−0.01936(27)	437.0(55)
O1b	0.33241(24)	0.69665(24)	−0.08462(45)	502.0(112)
O1b'	0.39441(29)	0.69968(28)	0.07463(49)	588.5(156)
O2b	0.34427(15)	0.52967(16)	−0.12296(27)	757.8(70)
O3b	0.41785(14)	0.53013(14)	0.07977(26)	715.6(68)

[a] Equivalent isotropic $U(eq)$ defined as one-third of the trace of the orthogonalized U_{ij} tensor.

Crystal Growth of B-N_2O_3: The sample (70% N_2O_3) crystallized at −115 °C on the diffractometer to give a light-blue solid. At −106 °C most of the substance, apart from a small residual amount in the tip of the capillary, was melted by carefully touching the sample with a finger. Crystallization started at the residual seed crystals and proceeded slowly through the sample; this was accompanied by a deepening in color. Rotation photographs showed the material to consist mainly of cubic N_2O_4. At the end of the solid column, a separated deep-blue section of 0.5 mm in length remained, which solidified at −108 °C. It was almost completely molten at −104.5 °C and recrystallized when cooled at a rate of 1 °C h^{-1}. An indigo-blue solid with colorless crystallites at its margins resulted. Rotation and oscillation photographs showed that a few crystallites of different sizes had formed. After two days at −106.5 °C a single crystal of B-N_2O_3 had formed.

X-Ray Single-Crystal Data Collection and Structure Analysis for B-N_2O_3: The apparatus and programs used are the same as described for A-N_2O_3. A cylindrical crystal with a diameter of 0.2 mm and a length of 0.5 mm was investigated. Unit cell parameters were determined from setting angles of 50 reflections ($24 \le 2\theta \le 43°$) and refined by least-squares methods. As the single crystal could be cooled to −160 °C without phase tranformation or destruction, we were able to collect data sets at six temperatures between −106.5 and −160 °C. At −160 °C a total of 2723 reflections were measured in the range $4 \le 2\theta \le 72°$ using the $\omega/2\theta$ scan technique. Three reflections, checked after every 47 reflections, showed intensity fluctuations less than 5%. Data were corrected for Lp effects; ψ-scan absorption data were taken at the end of the data collection (min./max. transmission 0.762/0.735); the correction method was that of a pseudo-ellipsoid in XEMP [16]. Systematic reflection absences and structure solution by direct methods led to space group $P2_12_12_1$. Refinement of 47 parameters by full-matrix least-squares methods resulted in a final $R1$ value of 0.023 for all reflections. For details of data collection, see Table 1. Fractional atomic coordinates and equivalent isotropic displacement parameters are given in Table 3.

Table 3. Fractional atomic coordinates and equivalent isotropic displacement parameters (pm^2) for B-N_2O_3 at −160 °C.

atom	x/a	y/b	z/c	U(eq) [a]
N1	0.42740(9)	0.99671(7)	0.65537(6)	260.4(10)
N2	0.10128(9)	0.86081(6)	0.62596(5)	195.4(8)
O1	0.44185(9)	1.10987(6)	0.55751(5)	310.6(10)
O2	−0.00655(8)	0.91536(6)	0.50829(5)	261.7(9)
O3	0.02856(10)	0.73428(6)	0.71958(6)	325.8(11)

[a] Equivalent isotropic $U(eq)$ defined as one-third of the trace of the orthogonalized U_{ij} tensor.

Thermal-Expansion Tensors: Thermal-expansion tensors were calculated according to the procedure of Jessen and Küppers [18] by least-squares methods for 50 reflections with 2θ values of 20–30° for phase A and 24–43° for phase B. The tensor components α_{ij} are given in Table 4.

Table 4. Tensor components of thermal expansion ($10^{-6}\,K^{-1}$) for A- and B-N_2O_3.

Phase	T/°C	α_{11}	α_{22}	α_{33}
A	−120 to −170	238.8(22)	238.8(22)	103.5(26)
B	−115 to −140	188.5(48)	199.7(55)	198.5(52)
	−140 to −160	123.9(51)	168.3(58)	159.2(56)

Results and Discussion

Phase Relationships and Crystal Growth: Using both DTA and powder diffraction we observed, after quenching N_2O_3/N_2O_4 samples to temperatures below −160 °C, an irreversible reaction at −150 °C, an enantiotropic phase transition at −125 °C, and the eutectic melting of N_2O_3 at -108 ± 2 °C, in agreement with previous thermal measurements.[19]

Phase E could be obtained exclusively by quenching samples to temperatures below −160 °C. It disappeared at −150 °C; this was accompanied by an exothermic signal in the DTA while cubic N_2O_4 together with phase B of N_2O_3 formed (cf. Fig. 2). These observations are best explained in terms of the existence of at least one new oxide below −150 °C with a composition between that of N_2O_3 and N_2O_4. The endothermic signal observed by DTA upon heating to −125 °C corresponds to the transition from B-N_2O_3 to A-N_2O_3.

For samples with rather high ($\ge 70\%$) or low ($\le 40\%$) N_2O_3 concentrations, the kinetics of nutrient formation became dominant. Samples with N_2O_3 concentrations of 20–40% showed a high tendency to form A-N_2O_3, which could be utilized for crystal growth. These samples were solidified at −120 °C as polycrystalline materials and crystals for X-ray diffraction were obtained by annealing 0.1–0.5 °C below the melting point. However, we did not observe the marked transition reported by Reed and Lipscomb,[10] in which single crystals of A-N_2O_3 were transformed into a powder when cooled below −125 °C. In our investigation single crystals could be cooled to −170 °C without undergoing a phase transition.

For crystal growth of B-N_2O_3 we used the peculiar behavior of samples with N_2O_3 concentrations greater than 70%. In this case phase A did not crystallize from the melt. A single crystal of phase B was grown after N_2O_3 had been enriched locally. This is probably the reason why the low-temperature modification crystallized a few degrees below the melting point.

Structures: B-N_2O_3 crystallizes in space group $P2_12_12_1$ with one molecule in the asymmetric unit. Distances and angles for B-N_2O_3 and A-N_2O_3 are compared in Table 5.

Table 5. Selected bond lengths (pm) and angles (°) for B-N_2O_3 and A-N_2O_3 (see Figs. 3(right) and 4 for atom labels).

B-N_2O_3			
N1–N2	189.0(1)	N2–N1–O1	105.11(4)
N1–O1	112.1(1)	N1–N2–O2	111.89(4)
N2–O2	120.6(1)	N1–N2–O3	119.53(4)
N2–O3	120.9(1)	O2–N2–O3	128.57(5)
A-N_2O_3, molecule a			
N1a–N2a	192.0(4)	N2a–N1a–O1a	101.19(26)
N1a–O1a	107.7(3)	N1a–N2a–O2a	115.50(22)
N2a–O2a	118.6(3)	N1a–N2a–O3a	116.04(22)
N2a–O3a	119.5(3)	O2a–N2a–O3a	128.43(25)
A-N_2O_3, molecule b			
N1b–N2b	191.3(3)	N2b–N1b–O1b	99.82(31)
N1b'–N2b	191.3(3)	N2b–N1b'–O1b'	100.96(34)
N1b–O1b	114.7(6)	N1b–N2b–O2b	122.01(25)
N1b'–O1b'	114.7(6)	N1b'–N2b–O2b	108.24(27)
N2b–O2b	118.6(3)	N1b–N2b–O3b	109.11(24)
N2b–O3b	119.5(3)	N1b'–N2b–O3b	122.82(28)

The high-temperature phase A of N_2O_3 crystallizes in a tetragonal unit cell with two molecules per asymmetric unit. Reflection conditions led to the assignment of space group $I4_1/a$, and structure solution by direct methods indicated disordered N_2O_3 molecules. Least-squares refinement of various disorder

models never converged. The apparent higher Laue symmetry $4/mmm$ of the diffraction pattern indicated twinning by merohedry.

If the volumes of twin components are equal, enhanced Laue symmetry of the resulting diffraction patterns occurs for twin operations that do not belong to the Laue class of the crystal. For crystal **2**, which displays nearly equal volumes of twin components (see Table 6), we in fact observed Laue class $4/mmm$ as reported by Reed and Lipscomb.[10] For crystal **1** with a nearly 1:3 ratio of twin components, the intensities of some reflections were obviously inconsistent with the apparent higher Laue class. Furthermore, $I4_1/a$ is one of the rare space groups for which discrepancies between the simulated Laue class of a twin and the extinction symbol can be recognized,[20] since there is no space group in Laue class $4/mmm$ that requires only the observed extinctions and no others.

Refinement with the mirror planes (110) or (100), as twin element, revealed one ordered molecule in the asymmetric unit and a second one with an NO moiety that was still disordered. A disorder model using similarity restraints for distances within the NO groups and for N2b–N1b and N2b–N1b′ converged at $R1 = 0.051$ for all reflections. A final Fourier difference map showed a maximum of $0.25\,e\,Å^{-3}$ and a minimum of $-0.16\,e\,Å^{-3}$.

In the following discussion, the ordered molecule is designated as molecule **a**, and the molecule that displays disorder of the NO unit as molecule **b**. A split model for O1b in molecule **b** (Fig. 3, left) yielded unreasonable displacement parameters for N1b, and bond lengths and angles disagreed significantly with those of the ordered molecule **a**. This result can be interpreted in terms of partial overlap of the two possible orientations of the molecule. Therefore we applied another model in which the entire NO group group was split (Fig. 3, right). The N–O bond lengths within the disordered group as well as the displacements

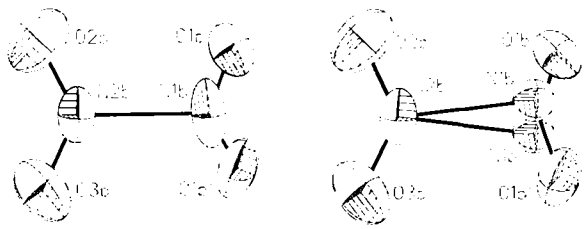

Fig. 3. Structure of the disordered molecule **b** in A-N_2O_3 with split models for O1b (left) and N1b and O1b (right). Displacement ellipsoids are drawn at the 50% probability level.

of N2b from N1b and N1b′ were given similarity restraints. All but the N atoms of the disordered NO group were refined anisotropically (see Fig. 3). The resulting N–N (191.3 pm) and N–O (114.7 pm) bond lengths (Table 5) compare reasonably well with those in molecule **a** (192.0 pm and 107.7 pm, respectively). The differences between these values can be attributed to the fact that the disorder model is still inadequate, since the centers of gravity of the disordered N atoms are too close to be sufficiently resolved by X-ray structure analysis. The NO_2 group is practically unaffected by disorder: relative orientation and size of the displacement ellipsoids are, within experimental error, equal to those of the ordered molecule.

Least-squares refinements yielded, for both crystals and for all temperatures studied, site occupation factors of about 0.54 and 0.46 for the positions of the disordered NO group (see Table 6). The fact that the site occupation factors are observed to be independent of temperature indicates a static disorder.

Table 6. Comparison of site occupation factors for O1 and of volume ratios of the twin domains for crystals **1** and **2** of A-N_2O_3.

Crystal	T/°C	Twin elements/%	Occupation for O1/%
1	−115	72:28	53:47
	−120	72:28	54:46
	−170	73:27	53:47
2	−120	58:42	55:45

Discussion of the Structures: The most remarkable features of the N_2O_3 molecule are the nearly perfect planarity and the long N–N distance (189.0 pm), which corresponds to a Pauling bond order of 0.2.[21] Deviations from planarity are small: N2 is displaced by 0.7 pm from the N1-O2-O3 plane, while O1 lies at 6.4 pm from this plane, owing to a 3.7° twist of the NO group out of the plane of the NO_2 unit. The N–O distances and O-N-O angle indicate partial NO^+ character of the NO unit and partial NO_2^- character of the NO_2 unit. The bond length of 112.1 pm for N1–O1 should be compared with 115 pm for NO[22] and 106.3 pm for NO^+,[23] and the bond length of 120.6 pm for N2–O2 with 119.7 pm for NO_2[24] and 124 pm for NO_2^-.[25] The angle of 128.6° is intermediate between 115° for NO_2^-[25] and 134.3° for N_2O_4.[8]

The small bond orders of 0.2 and 0.4 for the N–N bonds in N_2O_3 and N_2O_4, respectively, indicate the presence of unusual bonding. In addition to the long N–N bonds and the planarity of the molecule, N_2O_3 exhibits two remarkable features: the NO_2 group is rotated by about 3.8° within the molecular plane, towards the NO group, and the O1-N1-N2 angle (105.1°) is smaller than for comparable compounds like NOF (110°)[26] and NOCl (112.2°).[13] This decrease in angle results in an O1···O2 distance (263 pm) which is even shorter than in N_2O_4 (267 pm),[8] despite the longer N–N bond length (189.0 vs. 175.8 pm in N_2O_4).

The geometries of the N_2O_3 molecules that occur in different surroundings in the investigated phases show small deviations in details compared to the molecular shape determined from microwave investigations.[7] The N–N distance of 189.1 pm is slightly larger than that in the gas phase (186.4 pm).

Theoretical descriptions of the N–N bond are hampered by the weak interactions between the NO and NO_2 groups. An optimization of the N–N bond length with the CISD method, keeping all other internal coordinates fixed, led to an underestimation (183.0 pm).[27] The geometry of N_2O_3 calculated in a density functional study[28] is in better agreement with our experimental results, although the calculated N–N bond lengths were slightly overestimated as 191.5 and 193.6 pm, depending on the corrections for exchange used. However, these investigations neither explained the planarity of the molecule, nor the relatively short O1···O2 distance.

Comparison of bond lengths and angles of the ordered molecules of phase A and B reveals significant differences (Table 5). Additionally, the displacement ellipsoids of the high-temperature phase are considerably larger than those of the low-temperature phase as can be seen in Figure 4 and Tables 2 and 3. Bond

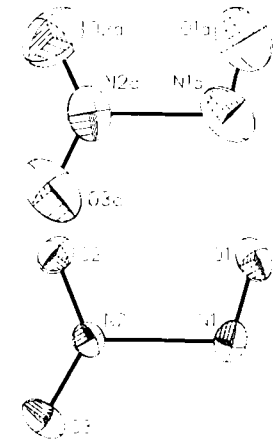

Fig. 4. Comparison of the ordered molecules of phase A (molecule **a**, top) and phase B (bottom). Displacement ellipsoids are drawn at the 50% probability level.

© VCH Verlagsgesellschaft mbH, D-69451 Weinheim, 1995 0947-6539/95/0106-0392 $ 30.00+.25/0 Chem. Eur. J. 1995, 1, No. 6

lengths and angles of phase A are affected by these large displacements, which cannot be corrected for libration[29] since the corresponding normal equations are underdetermined.

Concluding Remarks

Phase relationships in the system N_2O_3/N_2O_4 were investigated for samples of various compositions by means of the modified Guinier technique and differential thermal analysis. We observed powder diagrams of four phases, besides those of the stable cubic and the metastable monoclinic N_2O_4. The metastable phase F could be observed below $-135\,^{\circ}C$. Experimental results for phase E indicate the existence of at least one nitrogen oxide below $-150\,^{\circ}C$ having a composition between N_2O_3 and N_2O_4. Diffraction patterns of the previously reported phase D, which was observed only once,[11] could not be reproduced. Another phase previously called C[11] turned out to be A-N_2O_3 affected by texture effects. Phases A and B of N_2O_3 were established as stable phases from -108 to $-125\,^{\circ}C$ and -125 to $-150\,^{\circ}C$, respectively. Crystals of A-N_2O_3 and B-N_2O_3 were grown in situ on a diffractometer and investigated by X-ray single-crystal analysis. Both forms of N_2O_3 consist of almost planar molecules with extraordinarily long N–N bonds. The N–O distances and the O-N-O angles indicate a tendency of the nitroso–nitro compound to move towards a hypothetical nitrosyl–nitrite.

Received: February 15, 1995 [F88]

[1] L. J. Gay-Lussac, *Ann. Chim. Phys. (2)* **1816**, *1*, 400.
[2] J. Mason, *J. Chem. Soc.* **1959**, 1288.
[3] W. A. Yeranos, M. J. Joncich, *Mol. Phys.* **1967**, *13*, 263.
[4] J. C. Hisatsune, J. P. Devlin, *Spectrochim. Acta* **1960**, *16*, 401.
[5] H. Schultheiss, E. Fluck, *Z. Naturforsch.* **1977**, *32B*, 257.
[6] L. O. Andersson, J. Mason, *J. Chem. Soc. Chem. Commun.* **1968**, 99.
[7] A. H. Brittain, A. P. Cox, R. L. Kuczkowski, *J. Chem. Soc. Faraday Trans.* **1969**, *65*, 1963.
[8] A. Obermeyer, H. Borrmann, A. Simon, *Z. Kristallogr.* **1991**, *196*, 129.
[9] E. L. Varetti, G. C. Pimentel, *J. Chem. Phys.* **1971**, *55*, 3813.
[10] T. B. Reed, W. N. Lipscomb, *Acta Crystallogr.* **1953**, *6*, 781.
[11] A. Simon, J. Horakh, A. Obermeyer, H. Borrmann, *Angew. Chem.* **1992**, *104*, 325; *Angew. Chem. Int. Ed. Engl.* **1992**, *31*, 301.
[12] A. Simon, *J. Appl. Crystallogr.* **1971**, *4*, 138.
[13] A. Obermeyer, Dissertation, Univ. Stuttgart, **1992**.
[14] W. Biltz, W. Fischer, E. Wünneberg, *Z. Anorg. Allg. Chem.* **1930**, *193*, 351.
[15] Further details of the crystal structure investigation may be obtained from the Fachinformationszentrum Karlsruhe, D-76344 Eggenstein-Leopoldshafen (Germany), on quoting the depository number CSD-401604.
[16] G. M. Sheldrick, SHELXTL-PLUS, *Structure Determination Software*, Nicolet Instrument, Madison, WI, **1990**.
[17] G. M. Sheldrick, SHELXL-93, Göttingen, **1993**.
[18] S. M. Jessen, H. Küppers, *J. Appl. Crystallogr.* **1991**, *24*, 239.
[19] I. R. Beattie, S. W. Bell, A. J. Vosper, *J. Chem. Soc.* **1960**, 4796.
[20] E. Koch in *International Tables for Crystallography*, *Vol. C* (Ed.: A. J. C. Wilson), Kluwer Academic Publishers, Dordrecht, Boston, London, **1992**, p. 10.
[21] L. Pauling, *J. Am. Chem. Soc.* **1947**, *69*, 542.
[22] D. B. Keck, C. D. Hause, *J. Mol. Spectroscopy* **1968**, *26*, 163.
[23] R. W. Field, *J. Mol. Spectroscopy* **1973**, *47*, 194.
[24] N. N. Greenwood, A. Earnshaw, *Chemistry of the Elements*, 1st ed., Pergamon, Oxford, **1984**.
[25] M. I. Kay, B. C. Frazer, *Acta Crystallogr.* **1961**, *14*, 56.
[26] D. W. Magnuson, *J. Chem. Phys.* **1951**, *19*, 1071.
[27] S. A. Maluendes, A. H. Jubert, E. A. Castro, *J. Mol. Struct. (Theochem.)* **1990**, *204*, 145.
[28] A. Stirling, I. Papai, J. Mink, D. R. Salahub, *J. Chem. Phys.* **1994**, *100*, 2910.
[29] E. F. Maverick, K. N. Trueblood, THMA11, Los Angeles, **1987**.

  0947-6539/95/0106-0393 $ 30.00+.25/0